Journal of Controlled Release 358 (2023) 358–367

Contents lists available at ScienceDirect

Journal of Controlled Release

journal homepage: www.elsevier.com/locate/jconrel

A starch-based implant as a controlled drug release system: Non-invasive *in vivo* characterization using multispectral fluorescence imaging.

Golbarg Esfahani [a], Henrike Lucas [a], Frank Syrowatka [b], Karsten Mäder [a,*]

[a] Institute of Pharmacy, Martin Luther University Halle-Wittenberg, Kurt-Mothes-Straße 3, 06120 Halle (Saale), Germany
[b] Interdisciplinary Center of Materials Science, Martin-Luther-University Halle-Wittenberg, Halle (Saale), Germany

ARTICLE INFO

Keywords:
Fluorescence imaging
In vitro
In vivo
Release kinetics
NIR dyes
Starch
Biodegradable implants
Optical imaging

ABSTRACT

Solid implants are parenteral depot systems that can provide a controlled release of drugs in the desired body area over a few days to months. Finding an alternative for the two most commonly used polymers in the production of parenteral depot systems, namely Poly-(lactic acid) (PLA) and Poly-(lactide-*co*-glycolide) (PLGA), is of great importance due to their certain drawbacks. Our previous study showed the general suitability of starch-based implants for controlled drug release system. In this study, the system is further characterized and the release kinetics are investigated *in vitro* and *in vivo* by fluorescence imaging (FI). ICG and DiR, two fluorescent dyes with different hydrophobicity serving as a model for hydrophilic and hydrophobic drugs, have been used. In addition to 2D FI, 3D reconstructions of the starch implant were also used to assess the release kinetics in 3D mode. The *in vitro* and *in vivo* studies showed a fast release of ICG and a sustained release of DiR over 30 days from the starch-based implant. No treatment-related adverse effects were observed in mice. Our results indicate the promising potential of the biodegradable biocompatible starch-based implant for the controlled release of hydrophobic drugs.

1. Introduction

Parenteral controlled release drug delivery systems (CR-DDS) have gained significant attention during the last decades due to their high potential to improve drug therapy. CR-DDS can provide a constant concentration of drugs in the desired area of the body over several days, weeks, or even months. Currently, Poly-(lactic acid) (PLA) and Poly-(lactide-*co*-glycolide) (PLGA) are the most commonly used polymers in the pharmaceutical industry to produce parenteral depot systems [1–3]. However, these polymers degrade into acidic monomers which might lead to autocatalytic processes and drug degradation prior to release. Market products show often nonlinear release profiles with burst release or lag times [4–6]. Starch as a natural and abundant polymer with non-toxic and non-acidic degradation products might be a potential alternative for PLA and PLGA [7]. Starch is stable in a prolonged period of storage in the dry state. It is mostly used in solid preparations for oral delivery such as powders and tablets with various functions such as diluent, binder, disintegrant and lubricant [8–10]. Versatility in starch uses coupled with its low cost makes it an attractive excipient in the pharmaceutical industry [11]. Starch-based materials are already clinically used as bioresorbable medical products for providing hemostasis [12]. The biosafety of starch in different formulations is proven by several studies [13,14]. Despite all these advantages, there are certain limitations in using starch as the main component of a controlled release system. The most important drawback is its weak mechanical stability and the rapid biodegradation of starch by amylases in the body [15]. Chemical modification of starch has been widely investigated to slow down starch biodegradation and to improve its mechanical stability [8]. Physical modifications are simple, cost-effective and eco-friendly compared to chemical modifications [16]. In our previous study, a physically modified starch based implant was produced by means of high temperature and high pressure during the hot melt extrusion process. The appropriate mechanical properties of the system were proved by texture analysis. The *in vitro* release from the system was assessed by different methods. The results confirmed the general suitability of the system in providing a sustained release of a hydrophobic active substance over a few days to a few weeks [17]. As *in vitro* release kinetics might differ from *in vivo*, the aim of this study was to assess the release behavior from the implant and the fate of the implant *in vivo*. As far as we are concerned, no previous study has reported the fate of parenterally

* Corresponding author.
E-mail addresses: golbarg.esfahani@pharmazie.uni-halle.de (G. Esfahani), henrike.lucas@pharmazie.uni-halle.de (H. Lucas), frank.syrowatka@cmat.uni-halle.de (F. Syrowatka), karsten.maeder@pharmazie.uni-halle.de (K. Mäder).

https://doi.org/10.1016/j.jconrel.2023.05.006
Received 3 March 2023; Received in revised form 16 April 2023; Accepted 5 May 2023
Available online 12 May 2023

administered solid implant based on starch *in vivo*. There are only a few techniques to assess the *in vivo* release kinetics non-invasively. In a recent study conducted by Collantes et al., radiolabeling as a non-invasive method is used for intranasal implant studies development. However, this technique is very expensive and needs special facilities for the use of radioactive material [18]. Optical imaging (OI) is one of the most commonly used techniques in the visualization of *in vivo* processes. In contrast to radiolabeling which is based on ionizing radiation associated with potentially negative side effects, OI uses nonionizing radiation ranging from ultraviolet to infrared light that enables longterm or repetitive observations [19,20]. Due to the higher penetration depth, longer wavelengths are preferred. It requires the presence of a suitable fluorescent molecule with the following desired properties:

- absorption and emission at longer wavelengths for better tissue penetration of the light
- high quantum yield (high intensity)
- long-term stability (no bleaching)
- long-range of linear correlation between dye concentration and signal intensity

In this study, the release kinetics from starch implant is investigated by OI both *in vitro* and *in vivo*. The near-infrared (NIR) dyes ICG and DiR were loaded into the implants as examples of hydrophilic and hydrophobic molecules. The NIR dyes have the advantage of fast clearance from the body and minimal retention in nontargeted organs [21]. ICG is the only FDA approved NIR dye for clinical studies and DiR is widely used in preclinical studies [22–24]. The implants were injected subcutaneously (SC) in mice and evaluated over time with OI. Also, the possibility to quantify and assess the release kinetics by 3D reconstructions of implants was evaluated and compared to 2D OI.

2. Materials and methods

2.1. Materials

The fluorescent dye 1,10-Dioctadecyl-3,3,30,30-Tetramethylindotricarbocyanine Iodide (DiR), was purchased from Thermo Fisher Scientific Inc. (Waltham, MA, USA). The starch (MAIZE STARCH AMYLO N-400) was kindly provided by Roquette (Lestrem, France). Testing media was Phosphate Buffered Saline (PBS) (Ph. Eur.) plus 1% sodium dodecyl sulfate (SDS), adjusted to pH 7.4. SDS was purchased from Sigma Aldrich Chemie GmbH (Munich, Germany). Indocyanine green (ICG) was purchased from Carl Roth GmbH, Karlsruhe, Germany.

2.2. Preparation of implant

The implants were prepared by a hot melt extruder (HME), (ZE 5 ECO; Three-Tec GmbH; Seon; Swiss). Water was used as a plasticizer with a ratio of 1 g to 2 g of the starch. Water and starch were mixed gently and the mixture was used in the extruder. Extrusion die with a 0.3 mm diameter was used. The chamber heating zone's temperatures were 70, 80 and 90 °C. The samples were collected and stored in opaque falcon tubes between 4 and 8 °C.

2.3. Implant characterization

2.3.1. Thermogravimetric analysis

The samples' moisture content was assessed by thermogravimetric analysis with a TG 209 instrument (Netzsch, Selb, Germany). The samples were heated up to 105 °C at a heating rate of 10 K/min and kept at this temperature for 90 min. Nitrogen was used as a flushing gas with a flow rate of 20 ml/min.

2.3.2. Differential scanning calorimetry

DSC measurements were recorded with a Mettler Toledo DSC 823e module (Mettler Toledo, Gießen, Germany) in standard aluminium sample pans. Every sample was kept at 25 °C for 2 min and then heated up to 150 °C with a 10 K/min heating rate. All samples were kept at 150 °C for 1 min and then cooled down to 25 °C and kept at this temperature for 2 min and then heated up again up to 150 °C with a 10 K/min heating rate. Data recording and processing of the first heating cycle were carried out with the software STARe V15.00 (Mettler Toledo, Gießen, Germany) as no thermal event was observed during the cooling and second heating cycles.

2.3.3. Scanning electron microscopy

The samples were broken into tiny pieces and the breakage surface was imaged using an XL 30 ESEM device, with a GSE detector and 12.0 kV electron beam, in wet modules, under low vacuum and pressure of 1 mbar to prevent possible changes in the internal structure of the system due to the fast water evaporation.

2.4. ICG loaded implant preparation

The implants were prepared by a hot melt extruder (HME), (ZE 5 ECO; Three-Tec GmbH; Seon; Swiss). Fluorescent dye, ICG, which was dissolved in water, was added to the starch to reach the concentration of 8 μg per g of the implant. Water was used as a plasticizer with a ratio of 1 g to 2 g of the starch. Water and starch were mixed gently and the mixture was used in the extruder. Extrusion die with a 0.3 mm diameter was used. The chamber heating zone's temperatures were 70, 80 and 90 °C. The samples were collected and stored in opaque falcon tubes between 4 and 8 °C.

2.5. DiR loaded implant preparation

The implants were prepared by a hot melt extruder (HME), (ZE 5 ECO; Three-Tec GmbH; Seon; Swiss). Fluorescent dye, DiR, was dissolved in Ethanol. The required amount was added to the starch to reach a concentration of 1.5 μg per g of the implant. The organic solvent was evaporated under the vacuum. Water was used as a plasticizer with a ratio of 1 g to 2 g of the starch. Water and starch were mixed gently and the mixture was used in the extruder. Extrusion die with a 0.3 mm diameter was used. The chamber heating zone's temperatures were 70, 80 and 90 °C. The samples were collected and stored in opaque falcon tubes between 4 and 8 °C.

2.6. DiR loaded MCT oil as a control

A solution of the DiR with the same concentration of 1.5 μg per g of MCT oil was prepared by simply dissolving the required amount of DiR in MCT oil. This solution was used as a control for DiR implant to confirm that the prolonged release of DiR from DiR implant is not due to retention of the dye in the surrounding tissue at the injection site.

2.7. E-beam sterilization

Electron beam irradiation was chosen as the sterilization process. The extrudates were irradiated by a 10 MeV linear accelerator MB 10–30 MP (Mevex, Stittsville, Ontario, Canada) on a moving tray (95 cm/min). The total dose of 25 kGy was achieved by administering two separate doses of 12.5 kGy each (beam current 250 mA, PPS = 450 Hz).

2.8. In vitro release studies

2.8.1. ICG release

The extrudates were cut into implants with 0.5 cm length and 0.3 mm diameter ($n = 6$). Each implant was put in one well of a six-well plate. PBS was used as a release media (4 ml in each well). The plate was slightly agitated in a shaker with light protection (Memmert GmbH + Co. KG, Schwabach, Germany) at 37 °C. Before each imaging, the

media was withdrawn completely. After the imaging, an appropriate volume of fresh PBS was replaced. First imaging was carried out from the implant in a dry state as a D0 time point and then repeated on D1/2/4/7.

2.8.2. DiR release

The extrudates were cut into implants with 0.5 cm length and 0.3 mm diameter ($n = 6$). Each implant was put in one well of a six-well plate. PBS plus 1% SDS was used as a release media to ensure the sink condition (4 ml in each well). The plate was slightly agitated in a shaker with light protection (Memmert GmbH + Co. KG, Schwabach, Germany) at 37 °C. Before each imaging, the media was withdrawn completely. After the imaging, an appropriate volume of fresh PBS plus 1% SDS was replaced. First imaging was carried out from the implant in a dry state as a D0 time point and then repeated on D1/2/4/7/10/14/17/21/24/28/31.

2.9. In vivo release studies

All animal experiments were approved by local authorities of Saxony-Anhalt, Germany, and complied with the guidelines of the Federation for Laboratory Animal Science Associations (FELASA) [25,26]. Hairless SKH1 mice with albino background were used to avoid fluorescence signal absorption and scattering by hairs. Mice were kept under controlled standard conditions (12 h day/night cycle, 24 °C) in individually ventilated cages in groups of 2–5 individuals with food and water *ad libitum*. Mice condition and body weight were monitored over time. After the experiment, the mice were sacrificed by cervical dislocation. Tissue at the injection site was fixed in 5% formalin in PBS for histology investigations (FFPE–formalin fixed paraffin embedded). The FFPE samples were cut into 3 to 4 μm thin tissue sections on a microtome (Leica Biosystems Nussloch GmbH, Nussloch, Germany). Afterwards, dewaxation and rehydration were performed in a decreasing alcohol series from xylene to water. Standard hematoxylin and eosin (HE) staining followed using a ready-to-use hematoxylin solution and an acetic-acidic 0.1% eosin solution. After a series of increasing alcohol solutions from water to xylene, the sections were covered by Entellan© finally. Microscopic analysis was performed on an Axio Lab microscope (Zeiss, Jena, Germany) using a bright field. Pictures were taken with software Axiovision and camera Axiocam MRm (both Zeiss, Jena, Germany) in 10- to 40-fold magnification (Fig. 13) [27].

2.9.1. ICG implant in vivo release

The implants with 0.5 cm length and 0.3 mm diameter were implanted in anaesthetized mice subcutaneously (SC) in the loose skin overlying the upper back and shoulders into the nuchal fold. A 24G needle filled with an implant was inserted firmly through the skin from caudal to cranial. When correctly placed, the extrudate was pushed out of the needle with an ethanol sanitized plunger made out of wire. Finally, the needle was slowly removed by pulling back with one hand under slight skin fixation using the thumb and forefinger of the other hand ($n = 7$). First imaging was carried out directly after the SC injection of the samples as a D0 time point and then repeated on D1/2/4/7.

2.9.2. DiR implant in vivo release

The implants with 0.5 cm length and 0.3 mm diameter were implanted in anaesthetized mice SC in the loose skin overlying the upper back and shoulders into the nuchal fold. The 24G needle filled with an implant was inserted firmly through the skin from caudal to cranial. When correctly placed, the extrudate was pushed out of the needle with an ethanol sanitized plunger made out of wire. Finally, the needle was slowly removed by pulling back with one hand under slight skin fixation using the thumb and forefinger of the other hand ($n = 7$). First imaging was carried out directly after the SC injection of the samples as a D0 time point and then repeated on D1/2/4/7/10/14/17/21/24/28/31.

2.9.3. DiR solution (MCT) in vivo release

The DiR solution (10 μL) was injected subcutaneously (SC) in the loose skin overlying the upper back and shoulders into the nuchal fold ($n = 3$). First imaging was carried out directly after the SC injection of the samples as a D0 time point and then repeated on D1/2/4/7.

2.10. Fluorescence imaging: data acquisition and analysis

For *in vitro* and *in vivo* fluorescence imaging (FI), the IVIS Spectrum FI system (PerkinElmer, Inc., Waltham, MA, USA) was used. Mice were anaesthetized by inhalation anaesthesia (initially: 2.5% *v*/v isoflurane (Forene, Abbott, Wiesbaden, Germany) in oxygen at 3 L/min, maintenance: 2.5% at 0.3 L/min) in an XGI-8 narcosis system, Caliper Life Sciences (Runcorn, Cheshire, UK) and imaged at 37 °C in the IVIS Spectrum FI system. The FI system was equipped with a 150 W quartz wolfram halogen lamp. Grayscale and FI signals were recorded with a 4.1 megapixel (2048 × 2048) CCD camera at a working temperature of −90 °C. Analysis of *in vitro* and *in vivo* images was performed with Living Image® software, version 4.7.3.20616, PerkinElmer, Inc. (Waltham, MA, USA). The imaging was done with an epi-illumination system in which the source and detectors reside on the same side of the tissue. The respective experimental parameters are presented in the supplements (Table S1). For both *in vitro* and *in vivo* studies, the region of interest (ROI) was defined as an ellipsoid area with dimensions of a longitudinal axis of 1.2 cm and a transversal axis of 0.6 cm. Total radiant efficiency (TRE) was assessed. It takes into account the exposure time and area, quantity of detected photons, a fixed spatial angle (steradian) and the

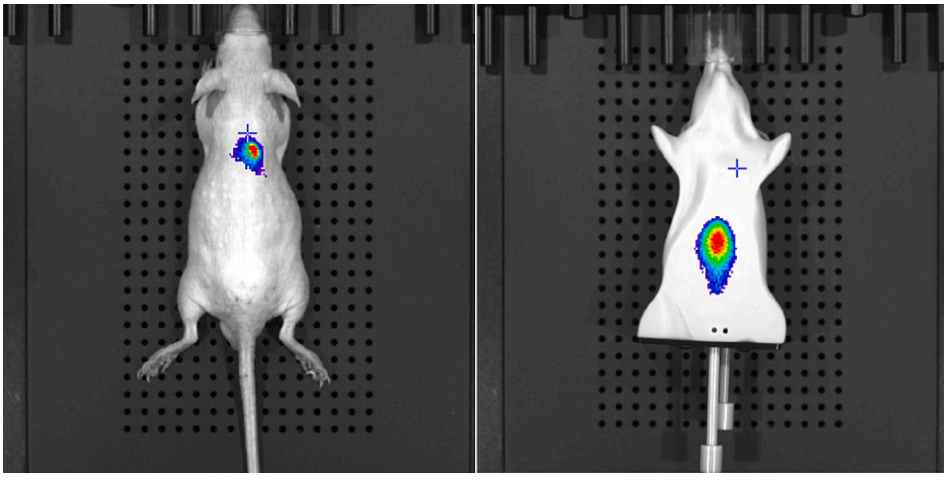

Fig. 1. Image examples obtained with the FLIT sequences acquired in dorsal (mouse) and ventral (mouse phantom) positions.

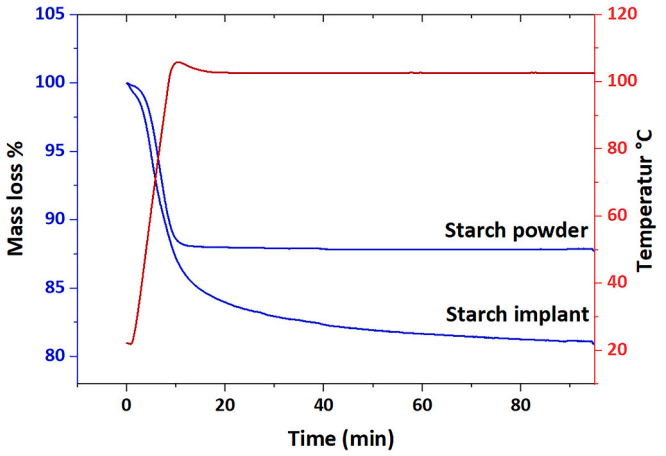

Fig. 2. Curves of different sample mass loss (in blue) and temperature of the chamber (in red) plotted against time. The blue curves show the average value for each sample ($n = 3$). (For interpretation of the references to colour in this figure legend, the reader is referred to the web version of this article.)

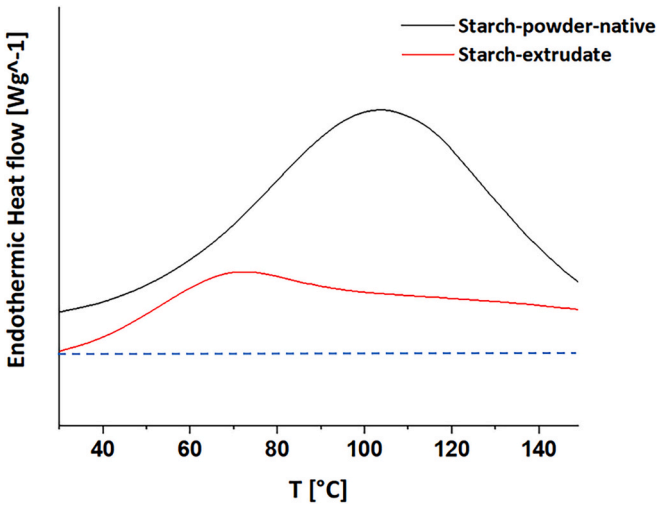

Fig. 3. Differential scanning thermograms of starch powder before (Black) and after (Red) the extrusion process. (For interpretation of the references to colour in this figure legend, the reader is referred to the web version of this article.)

exposure intensity, allowing quantitative comparisons between different implants, mice and time points. To determine the background signal of the mouse body, a region of interest (ROI) was set on the untreated area at the lower back in the lumbar-sacral region of each mouse. The TRE of the untreated area (background area) was subtracted from the TRE of the injection area. In principle, quantification in fluorescence imaging can be approached only through a combination of light transport modelling, data normalization and calibration. In this study, the approach of normalized data was used as the signal has travelled more or less the same tissue path length and the impact of the normalization is to approximately cancel out geometrical and heterogeneity effects that cannot be controlled experimentally [9–11]. For the normalization, TRE at D0 was defined as 1.

2.11. 3D reconstruction of the implant

The Imaging Wizard was used to acquire the Fluorescent Tomography (FLIT) sequence. Always four points (surrounding the injection site) were chosen as the transillumination locations. The low lamp level was used to acquire the FLIT sequences. The surface of the mouse or phantom mouse (XFM-2×) was generated automatically by the software. The XFM-2× Phantom Mouse is made to mimic tissue properties. The colour of the surface of the phantom emulates the behavior of tissue autofluorescence [28]. The phantom mouse is a good tool to optimize the sample composition (*e.g.* dye concentration) and measuring conditions *in vitro* to prepare *in vivo* experiments. It was not made for *in vitro* release experiments in pharmaceutics. Best 3D reconstructions were obtained by Normalized Transmission Fluorescence (NTF) by manual reconstruction.

As can be seen in Fig. S1, there are two different holes in the mouse phantom. In order to simulate the subcutaneously injected implant the upper hole close to the surface of the mouse phantom (in ventral position) was used.

As for the *in vivo* studies the implants were injected in the loose skin overlying the upper back of the mice, the FLIT sequences were acquired with a dorsal position whereas a ventral position was used for mouse phantom (Fig. 1). For the measurement of the signal in 3D fluorescent sources, a 3D region of interest (ROI) with the dimensions of 5*5*10 mm was used. The fluorescence yield summed over the 3D ROI (Total pmol M^{-1} cm^{-1}) was calculated by the software automatically.

2.12. In vivo release 2D vs 3D

As DiR loaded implant showed a sustained release over a month, this implant was used to assess the possibility of using FLIT 3D reconstruction in the quantification of *in vivo* release. To ensure a linear concentration/intensity relation and to monitor the release at a later time point, two different concentrations of the DiR dye 1.5 and 50 μg/g were used. The implants were injected subcutaneously as mentioned previously and the mice were imaged with both epi-illumination (2D) and FLIT (3D). Imaging was performed directly after the injection as D0 and then repeated on D1/2/5/8/12/15/19/22/26/33/40 for 2D and on D2/5/8/12/15/19/22/26/33/40 for 3D. FLIT measurement on day 1 was not performed to prevent mice's long exposure to anaesthesia gas for three continuous days. The FLIT measurement takes longer than epi-illumination (2D).

3. Results and discussion

3.1. Thermogravimetric analysis

As can be seen in Fig. 2, starch powder showed a total mass loss of 12% which corresponds to the water content of the sample. The value is in the normal range of starch samples [29]. Looking at the starch implant TGA curve, it can be seen that, the system had a total mass loss of 20%. As before the extrusion process, water was added to the starch (1 g water to 2 g starch), it can be concluded that a significant part of the water is removed from the system during the extrusion process.

3.2. Differential scanning calorimetry

Figure 3 shows the DSC graph of starch powder and starch implant. The water evaporation peak can be seen in the DSC curve of the starch powder sample, with the maximum peak around 100 °C. As the starch implant is gelatinized during the extrusion process and later on retrograded during cooling of the implant at room temperature, a thermal transition peak of retrograded starch can be seen in the starch extrudate DSC curve with maximum peak around 69 °C [30].

3.3. Scanning electron microscopy (SEM)

The SEM image (Fig. 4) shows the broken surface of the implant. Looking closer at the breakage surface, it can be seen that the starch granules are gelatinized and the content of the granules is leaked out.

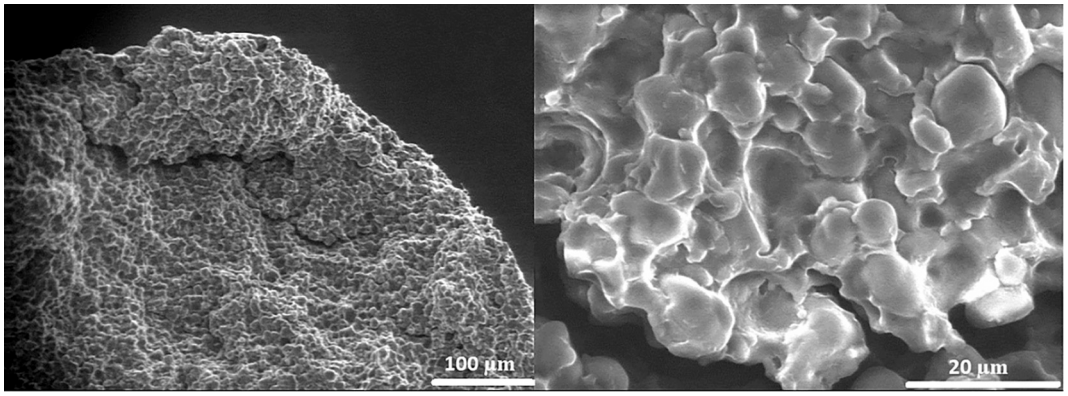

Fig. 4. SEM image of the broken surface of the implant: (**a**) scale bar shows 100 µm; (b) scale bar shows 20 µm.

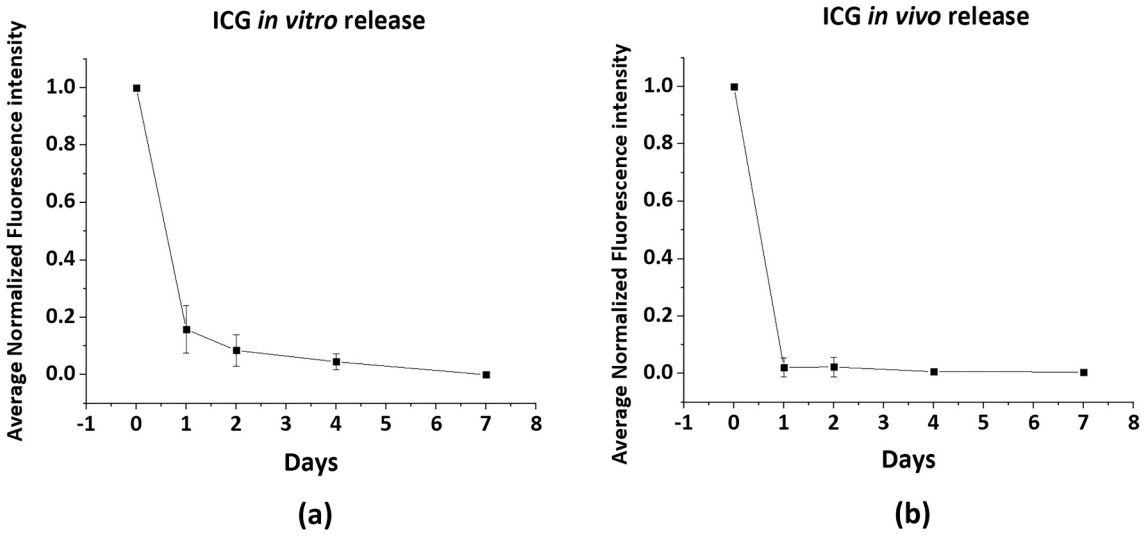

Fig. 5. Kinetics of ICG signals from starch extrudates after: (**a**) incubation in buffer, (*in vitro)*; (**b**) injection into mice, (*in vivo);* (Mean ± SD, $n = 7$).

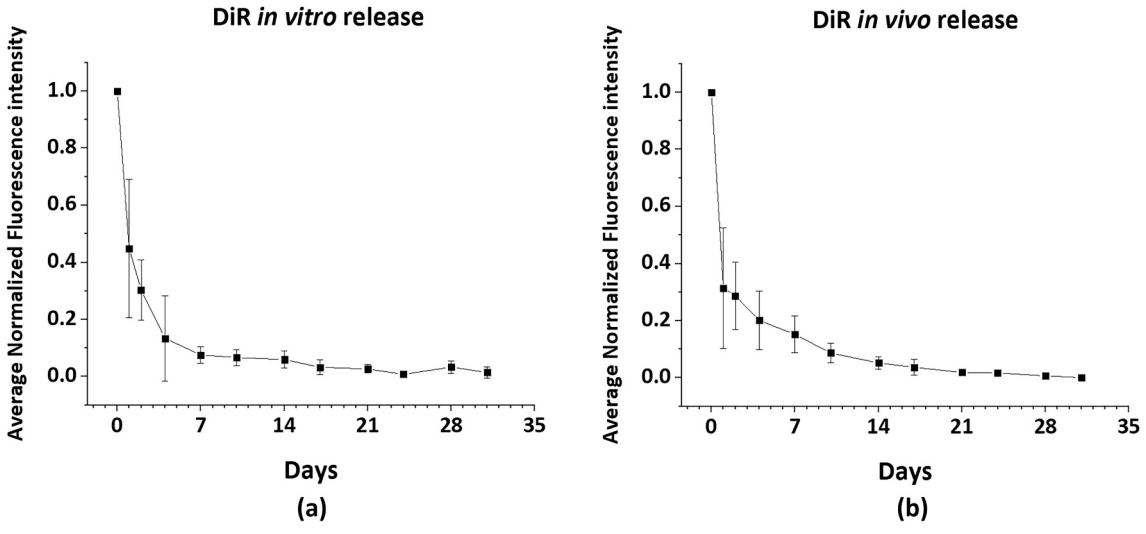

Fig. 6. Kinetics of DiR signals from starch extrudates after: (**a**) incubation in buffer, (*in vitro)*; (**b**) injection into mice, (*in vivo);* (Mean ± SD, $n = 7$).

3.4. ICG in vitro/in vivo release (2D)

As can be seen in Fig. 5, the signal intensity is significantly decreased after the first day, which proves the fast release of ICG from the system both *in vitro* and *in vivo*. The *in vitro* results are in line with the results of our previous publication, where Electron Paramagnetic Resonance (EPR) was implemented to assess the mobility of the drug models (spin probes) and polarity inside the system. This study showed that the water

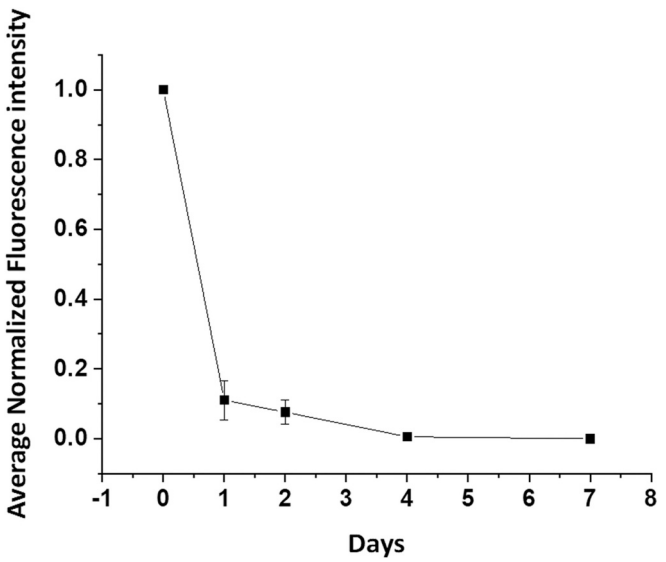

Fig. 7. Kinetics of DiR signals after administration of a DiR loaded MCT solution (Mean ± SD, $n = 3$).

penetration into the starch implant is very fast (a few minutes). Therefore, the existence of water inside the system leads to fast release of hydrophilic substance by diffusion from the system. Tempol as a model of a hydrophilic drug showed fast solubilization after buffer exposure and a similar release behavior as ICG *in vitro* [17]. FI as a more sensitive method than the EPR, enabled us to assess the biodegradability of the implant and release of a hydrophilic drug model from the implant *in vivo* non-invasively.

3.5. DiR in vitro/in vivo release (2D)

Figure 6 shows the *in vitro* and *in vivo* release of the lipophilic dye DiR. As can be seen in the figure, DiR signals could be detected over a period of 30 days. Therefore, compared to ICG, the release time of DiR is much longer. Most part of the DiR dye is released from the system over two weeks both *in vitro* and *in vivo*. The results are in line with the results of our previous *in vitro* EPR study, where Tempol Benzoate (TB) as a model of a hydrophobic drug showed a sustained release over two weeks from starch implant [17].

The *in vitro* and *in vivo* release profiles of DiR are very similar, which was not expected prior to the experiments. After 4 weeks, the experiment was finished and the implantation side was inspected *ex vivo*. The implant was completely degraded after 4 weeks, as no residue of the implant could be observed in any of the mice's tissue at the injection site macroscopically. *In vitro*, the starch extrudate was still present as a monolithic extrudate after 4 weeks. These findings suggest a complete degradation of the starch *in vivo* by enzymes, most likely amylases. Amylases are produced not only by salivary glands, pancreas and liver but also by other tissues and exist in serum at a normal level. The amylose and amylopectin molecules of starch are broken down into dextrins by these enzymes. The dextrins will be further on degraded to fermentable sugars, mainly maltose but some glucose as well [15]. Because of the different behavior *in vitro* and *in vivo*, nonenzymatic hydrolysis is not the major mechanisms of starch degradation *in vivo*. This is in contrast to PLA and PLGA implants, where (autocatalytic) hydrolysis is the major mechanism for polymer degradation.

3.6. DiR in MCT as a control

A possible artifact for the observed kinetics of the DiR could be an intrinsic strong association of the dye with the surrounding tissue. In this case, the DiR would remain for prolonged times at the side of injection (suggesting a "controlled release"), even after the administration of a solution. Therefore, an oily solution of DiR in MCT was injected as a control. As can be seen in Fig. 7, DiR signals were detectable for four days. This finding confirms that the DiR signals observed 4 weeks after implantation of the starch extrudates are due to the controlled release properties of the starch matrix and no the intrinsic properties of the DiR dye.

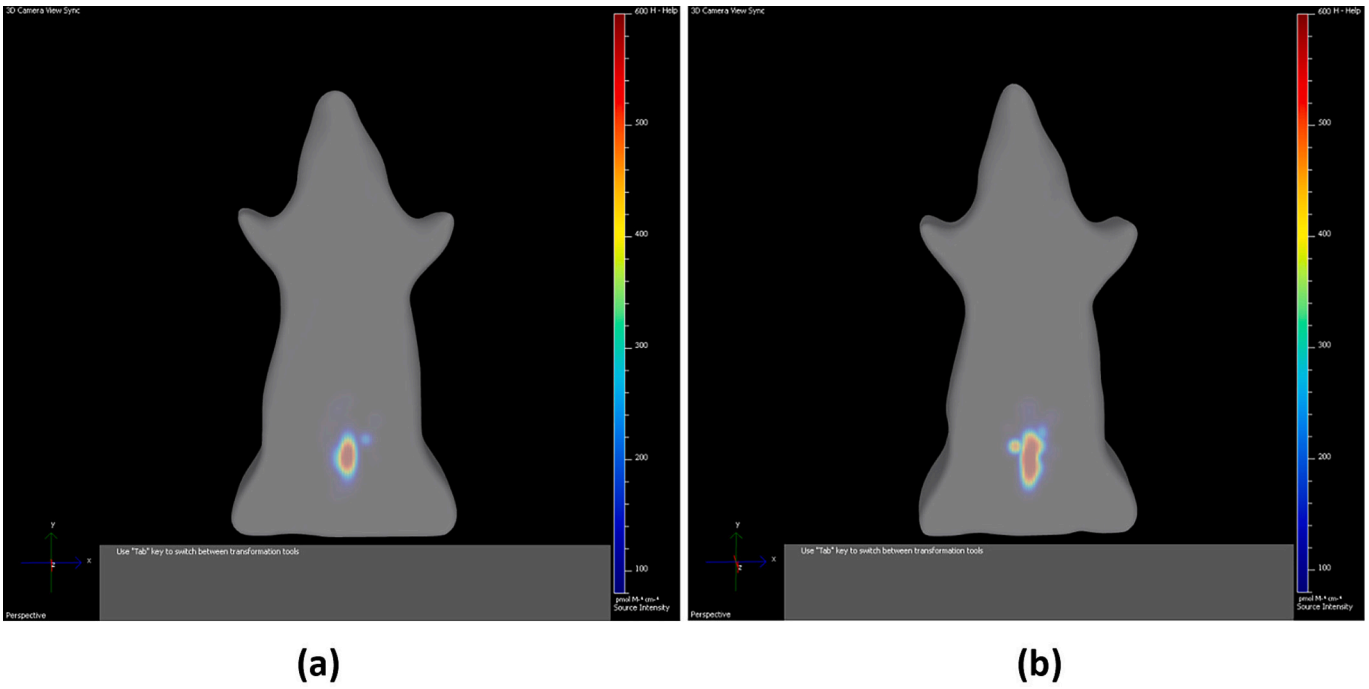

Fig. 8. The 3D reconstruction of the ICG loaded implant with different dimensions in the mouse phantom: (a) Implant with a diameter of 0.3 mm and length of 5 mm; (b)) Implant with a diameter of 0.3 mm and length of 10 mm.

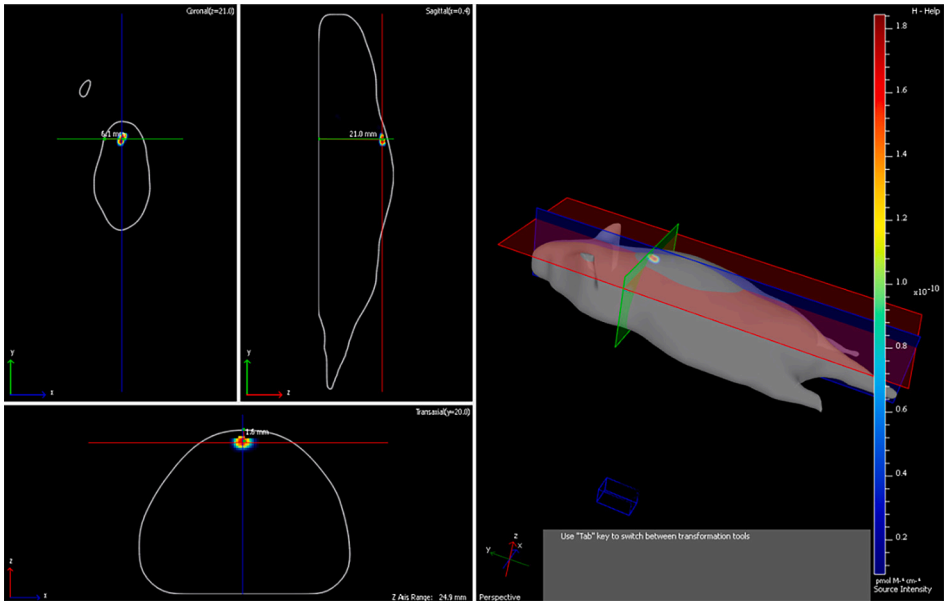

Fig. 9. The 3D reconstruction of the DiR loaded implant subcutaneously injected in the mouse.

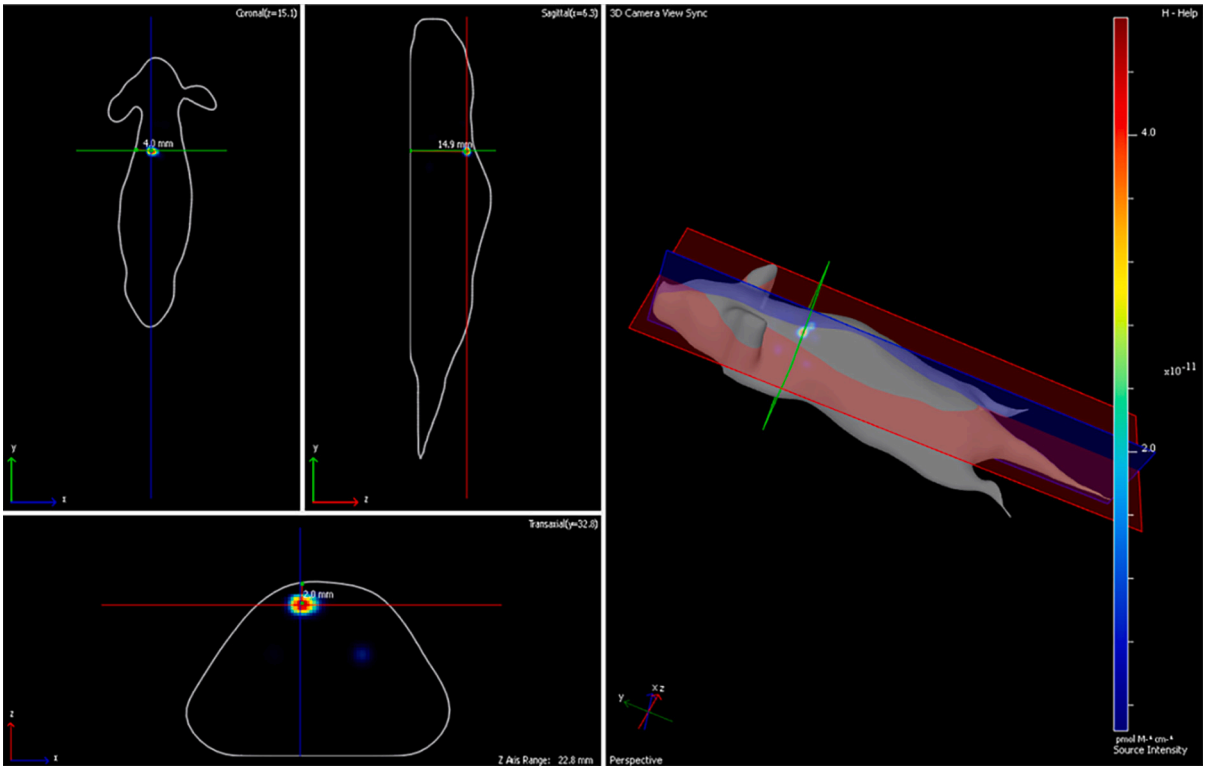

Fig. 10. The 3D reconstruction of the ICG loaded implant subcutaneously injected in the mouse.

3.7. 3D reconstruction of the implant

3D reconstruction of the fluorescent sources has been widely used in optical imaging. Several studies have demonstrated the positive correlation between the fluorescence signal intensity and tumor weights and volume (in our case size of the implant) [31–35]. In this study, this method was used to assess the fate of the fluorophore-loaded implant and the release of the fluorescent dyes as drug models from this implant. A possible problem in the 3D reconstruction of the fluorescent signal is the appearance of the artifacts due to model mismatch and out-of-plane effects [36]. Implants with different diameters were evaluated to assess the positive correlation between the fluorescence signal intensity and implant size and also to discriminate between the signal responsible for the implant and the artifacts. Fig. 8 shows the 3D reconstruction of the ICG loaded implants with different dimensions in the mouse phantom.

Figs. 9 and 10 show the 3D reconstructions of the SC injected implants in mice.

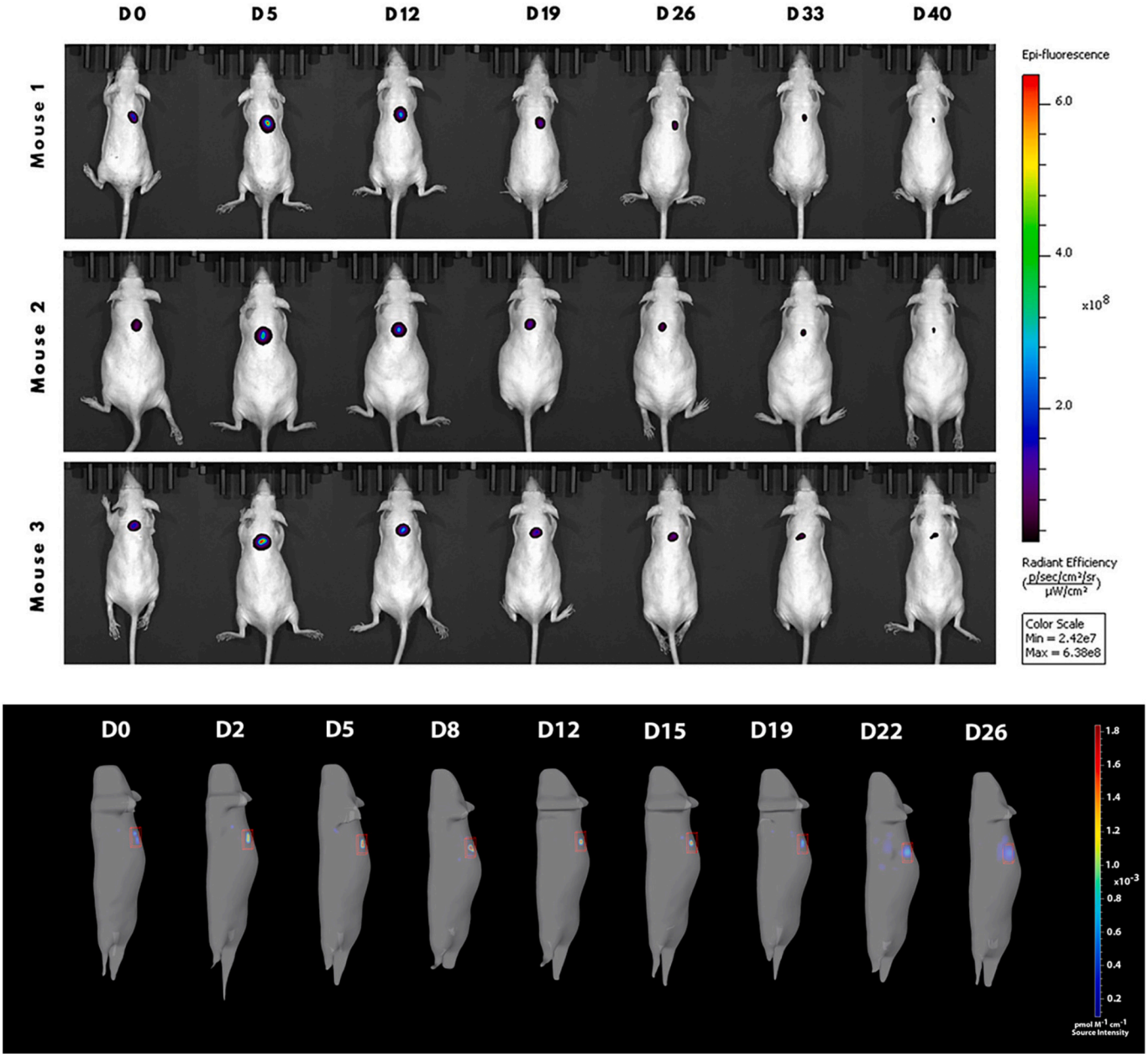

Fig. 11. Optical Images of DiR loaded starch implants: 2D imaging (Top), 3D reconstruction of the mouse 2 (Bottom).

3.8. *In vivo release 2D vs 3D*

Best 3D reconstructions are achieved with high signal intensity. It was expected that with the lower concentration of the dye (1.5 µg/g), the 3D measurement was only possible for a short period. We are aware about the risk of having nonlinear concertation / intensity relations for the higher concentration (50 µg/g) in the initial release period due to quenching effects, but nethertheless we did also use this concentration to prolong the overall measurement period *in vivo* in the 3D mode which is less sensitive compared to the 2D measurement. We also applied the lower DiR concentration of 1.5 µg/g which is in the linear region and avoids quenching problems. For the higher concentration of 50 µg/g we expected to see initially a period of increase in signal due to the quenching effect and then a decrease in signal intensity with the same behavior as an implant with 1.5 µg/g dye concentration. Fig. 11 shows the changes in fluorescent intensity assessed by 2D imaging and 3D reconstructions of the implant in mouse 2.

As can be seen in Fig. 11, the sensitivity of the device in epi-illumination (2D) is much higher than FLIT (3D). Because of this, the dye release can be assessed for a significantly longer period by 2D imaging in comparison to 3D reconstruction. Considering 2D images, the signal could be detected for 40 days. In contrast, 3D reconstruction of the implant was only possible for 33 days. Despite the limitation in sensitivity of the device, as can be seen in Fig. 12, the *in vivo* release curve obtained by 3D reconstructions matches the data obtained by 2D imaging until day 20. On day 25 an increase in signal intensity was observed in 3D probably due to artifacts which are formed in low concentrations of the dye close to the sensitivity limit of the device. Therefore applicable dye concentration range is much more limited in 3D mode data acquisition in comparison to 2D mode. This fact proves the need to use 2D measurements always as the established control method.

3.9. *Tolerability of the treatment, body weight and histology*

All treatments were well tolerated and no treatment-related adverse

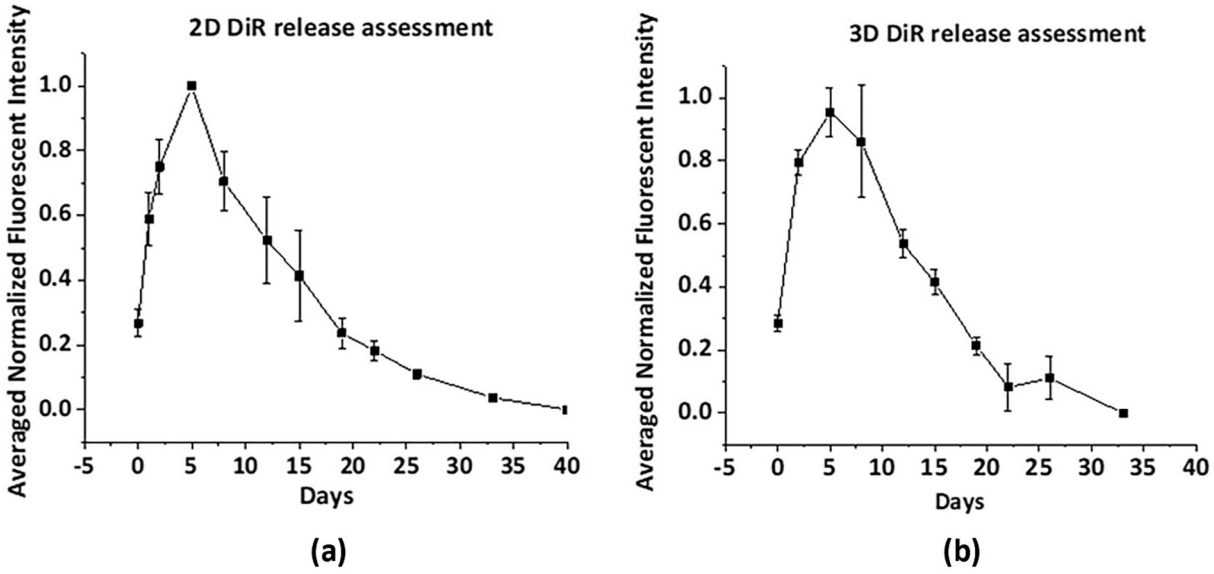

Fig. 12. Quantification of DiR signals detected *in vivo* (initial DiR concentration, 50 μg/g): (**a**) Quantification done by 2D images (epi-illumination). Error bars after day 20 are within the symbols; (**b**) Quantification done by 3D reconstructions (Mean ± SD, $n = 3$). A high DiR concentration was used to enable 3D measurements for prolonged times. The initial increase in signal intensity is due to the decrease of quenching effects.

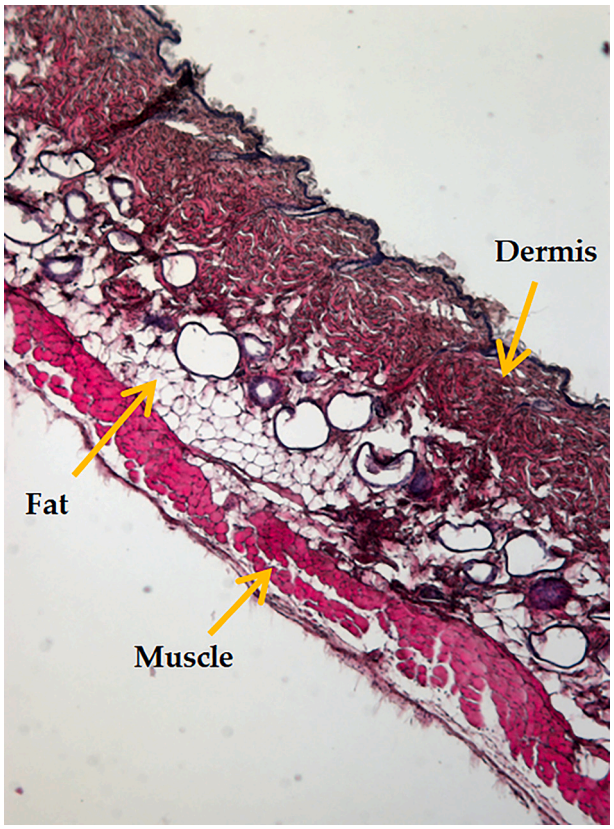

Fig. 13. The surrounding tissue of the injection site stained with hematoxylin–eosin (H&E).

effects were observed. The body weight of all mice involved in the study was either constant or increasing. Histological samples of the injection site were rated as normal (Fig. 13).

4. Conclusion

In this study, the *in vitro* and *in vivo* release from starch-based implants is investigated. The model compounds, namely ICG as a model of the hydrophilic drug and DiR as a model of a hydrophobic drug were loaded into the implants to assess the release kinetics by FI. The starch implants were injected SC in mice for further evaluation by FI. No inflammation or adverse effects were observed at the injection site. The ICG showed a fast release from the formulation both *in vitro* and *in vivo,* while DiR was released over 30 days. These results are in line with our previous study, where the EPR, as a non-invasive method, was utilized to assess the *in vitro* release kinetics from the formulation and water penetration into the implant using spin probes as model compounds. EPR data demonstrated the fast water penetration into the starch-based implant leading to the fast release of hydrophilic compound (Tempol) and sustained release of hydrophobic compound (Tempol Benzoate) *in vitro* [17]. In addition to the 2D FI, the 3D reconstruction of the implant was used to assess the release kinetics in 3D. The results of *in vivo* DiR release obtained by 3D reconstructed implant match the results obtained by 2D imaging. In this study, the 3D reconstruction was used for a very small implant with a regular shape. This can be expanded to the use of 3D reconstruction to assess the release kinetics in 3D mode from *in vivo* forming implants in future. After sacrificing the mice, the injection site was evaluated for the remaining part of the implant. The implant was completely degraded and no remaining part of the implant was detectable by unarmed eyes in any of the mice. In summary, the results prove the promising potential of the biodegradable biocompatible starch-based implant in forming a controlled release system for a hydrophobic drug.

Supplementary data to this article can be found online at https://doi.org/10.1016/j.jconrel.2023.05.006.

Funding

This research was funded by the European Social Fund (ESF) and the Federal State of Saxony-Anhalt.

Institutional review board statement

The study was conducted according to the guidelines of the

Declaration of Helsinki and approved by the Institutional Review Board of Saxony-Anhalt, Germany (42502–2-1500 MLU, date of approval: 18.07.2018).

CRediT authorship contribution statement

Golbarg Esfahani: Conceptualization, Methodology, Validation, Formal analysis, Investigation, Data curation, Writing – original draft. **Henrike Lucas:** Conceptualization, Methodology, Validation, Formal analysis, Investigation, Data curation, Writing – original draft. **Frank Syrowatka:** Methodology, Validation, Formal analysis, Investigation, Resources, Data curation. **Karsten Mäder:** Conceptualization, Methodology, Resources, Writing – review & editing, Supervision, Project administration, Funding acquisition.

Declaration of Competing Interest

The authors declare no conflict of interest.

Data availability

Data will be made available on request.

Acknowledgments

This study was supported by the IGS “Functional polymers” as a part of the AGRIPOLY program with funding from the European Social Fund (ESF). We would like to express our gratitude to Roquette (Lestrem, France) for providing us with the materials. We gratefully acknowledge the support of Dr. W. Knolle (Leibniz Institute of Surface Engineering) for the sterilization of the samples. Additionally, we would like to extend our appreciation to J. Kollan for all her help during the project and for teaching the H&E staining.

References

[1] C. Wischke, S.P. Schwendeman, Principles of encapsulating hydrophobic drugs in PLA/PLGA microparticles, Int. J. Pharm. 364 (2008), https://doi.org/10.1016/j.ijpharm.2008.04.042.
[2] Zoladex approved for prostate cancer, Drug. Ther. (NY) 20 (1990).
[3] D. Cuevas-Ramos, M. Fleseriu, Pasireotide: a novel treatment for patients with acromegaly, Drug. Des. Devel. Ther. 10 (2016), https://doi.org/10.2147/DDDT.S77999.
[4] A.G. Ding, S.P. Schwendeman, Acidic microclimate pH distribution in PLGA microspheres monitored by confocal laser scanning microscopy, Pharm. Res. (2008), https://doi.org/10.1007/s11095-008-9594-3.
[5] K. Mäder, B. Gallez, K.J. Liu, H.M. Swartz, Non-invasive in vivo characterization of release processes in biodegradable polymers by low-frequency electron paramagnetic resonance spectroscopy, Biomaterials. 17 (1996), https://doi.org/10.1016/0142-9612(96)89664-5.
[6] A. Schädlich, S. Kempe, K. Mäder, Non-invasive in vivo characterization of microclimate pH inside in situ forming PLGA implants using multispectral fluorescence imaging, J. Control. Release 179 (2014), https://doi.org/10.1016/j.jconrel.2014.01.024.
[7] M.A. Araújo, A.M. Cunha, M. Mota, Enzymatic degradation of starch-based thermoplastic compounds used in protheses: identification of the degradation products in solution, Biomaterials. 25 (2004), https://doi.org/10.1016/j.biomaterials.2003.09.093.
[8] M.A.V.T. Garcia, C.F. Garcia, A.A.G. Faraco, Pharmaceutical and biomedical applications of native and modified starch: a review, Starch/Staerke. 72 (2020), https://doi.org/10.1002/star.201900270.
[9] P.F. Builders, M.I. Arhewoh, Pharmaceutical applications of native starch in conventional drug delivery, Starch/Staerke. 68 (2016), https://doi.org/10.1002/star.201500337.
[10] R.C. Rowe, P.J. Sheskey, M.E. Quinn, Handbook of Pharmaceutical Excipients Sixth Edition, sixth edit, Rev. Des Nouv. Technol. l'Information., 2018.
[11] O.A. Odeku, Potentials of tropical starches as pharmaceutical excipients: a review, Starch/Staerke. 65 (2013), https://doi.org/10.1002/star.201200076.
[12] S. Jin, G. Yu, R. Hou, B. Shen, H. Jiang, Effect of hemodilution in vitro with hydroxyethyl starch on hemostasis, Med. Sci. Monit. 23 (2017), https://doi.org/10.12659/MSM.901588.
[13] A.J. Salgado, O.P. Coutinho, R.L. Reis, Novel starch-based scaffolds for bone tissue engineering: cytotoxicity, cell culture, and protein expression, Tissue Eng. (2004), https://doi.org/10.1089/107632704323061825.
[14] X. Zhang, Y. Liu, S. Gong, M. Li, S. Li, Y. Hemar, Probing the biotoxicity of starch nanoparticles in vivo and their mechanism to desensitize β-lactoglobulin, Food Hydrocoll. 135 (2023), 108166.
[15] H.D. Janowitz, D.A. Dreiling, The plasma amylase: source, regulation and diagnostic significance, Am. J. Med. 27 (1959) 924–935.
[16] S. Punia, Barley starch modifications: physical, chemical and enzymatic - a review, Int. J. Biol. Macromol. 144 (2020), https://doi.org/10.1016/j.ijbiomac.2019.12.088.
[17] G. Esfahani, O. Häusler, K. Mäder, Controlled release starch-lipid implant for the therapy of severe malaria, Int. J. Pharm. 622 (2022), https://doi.org/10.1016/j.ijpharm.2022.121879.
[18] J.A. Simón, E. Utomo, F. Pareja, M. Collantes, G. Quincoces, A. Otero, M. Ecay, J. Domínguez-Robles, E. Larrañeta, I. Peñuelas, Radiolabeled risperidone microSPECT/CT imaging for intranasal implant studies development, Pharmaceutics. 15 (2023) 843.
[19] D.A. Boas, D.H. Brooks, E.L. Miller, C.A. Dimarzio, M. Kilmer, R.J. Gaudette, Q. Zhang, Imaging the body with diffuse optical tomography, IEEE Signal Process. Mag. 18 (2001), https://doi.org/10.1109/79.962278.
[20] A.P. Gibson, J.C. Hebden, S.R. Arridge, Recent advances in diffuse optical imaging, Phys. Med. Biol. 50 (2005), https://doi.org/10.1088/0031-9155/50/4/R01.
[21] S. Zhu, R. Tian, A.L. Antaris, X. Chen, H. Dai, Near-infrared-II molecular dyes for Cancer imaging and surgery, Adv. Mater. 31 (2019), https://doi.org/10.1002/adma.201900321.
[22] FDA. Available online: https://www.accessdata.fda.gov/drugsatfda_docs/label/2006/011525s017lbl.pdf (accessed on 25.05.2022), (n.d.).
[23] J. Wang, F. Guo, M. Yu, L. Liu, F. Tan, R. Yan, N. Li, Rapamycin/DiR loaded lipid-polyaniline nanoparticles for dual-modal imaging guided enhanced photothermal and antiangiogenic combination therapy, J. Control. Release 237 (2016), https://doi.org/10.1016/j.jconrel.2016.07.005.
[24] H. Xin, X. Jiang, J. Gu, X. Sha, L. Chen, K. Law, Y. Chen, X. Wang, Y. Jiang, X. Fang, Angiopep-conjugated poly(ethylene glycol)-co-poly(ε-caprolactone) nanoparticles as dual-targeting drug delivery system for brain glioma, Biomaterials. 32 (2011), https://doi.org/10.1016/j.biomaterials.2011.02.044.
[25] J. Guillen, FELASA guidelines and recommendations, J. Am. Assoc. Lab. Anim. Sci. 51 (2012).
[26] H.M. Voipio, P. Baneux, I.A. Gomez De Segura, J. Hau, S. Wolfensohn, Guidelines for the veterinary care of laboratory animals: report of the FELASA/ECLAM/ESLAV joint working group on veterinary care, Lab. Anim. 42 (2008), https://doi.org/10.1258/la.2007.007027.
[27] M. Riehl, M. Harms, H. Lucas, T. Ebensen, C.A. Guzmán, K. Mäder, Dual dye in-vivo imaging of differentially charged PLGA carriers reveals antigen-depot effect, leading to improved immune responses in preclinical models, Eur. J. Pharm. Sci. (2018), https://doi.org/10.1016/j.ejps.2018.01.040.
[28] Perkin Elmer, Phantom Mouse, (n.d.). https://www.perkinelmer.com/product/xfm-2x-fluorescent-phantom-mouse-x-ray-133803 (accessed March 30, 2023).
[29] D.J. Thomas, W.A. Atwell, Eagan Press Handbook Series: Starches, Minnesota Eagan Press. Sch, St. Paul, 1999.
[30] H. Liu, L. Yu, Z. Tong, L. Chen, Retrogradation of waxy cornstarch studied by DSC, Starch/Staerke. 62 (2010), https://doi.org/10.1002/star.201000017.
[31] G. Choy, S. O'Connor, F.E. Diehn, N. Costouros, H.R. Alexander, P. Choyke, S. K. Libutti, Comparison of noninvasive fluorescent and bioluminescent small animal optical imaging, Biotechniques. 35 (2003), https://doi.org/10.2144/03355rr02.
[32] L. Liu, R.P. Mason, B. Gimi, Dynamic bioluminescence and fluorescence imaging of the effects of the antivascular agent Combretastatin-A4P (CA4P) on brain tumor xenografts, Cancer Lett. 356 (2015), https://doi.org/10.1016/j.canlet.2014.09.038.
[33] N. Zhao, C. Zhang, Y. Zhao, B. Bai, J. An, H. Zhang, J.B. Wu, C. Shi, Optical imaging of gastric cancer with near-infrared heptamethine carbocyanine fluorescence dyes, Oncotarget. 7 (2016), https://doi.org/10.18632/oncotarget.10031.
[34] I. Biancacci, Q. Sun, D. Möckel, F. Gremse, S. Rosenhain, F. Kiessling, M. Bartneck, Q. Hu, M. Thewissen, G. Storm, W.E. Hennink, Y. Shi, C.J.F. Rijcken, T. Lammers, A.M. Sofias, Optical imaging of the whole-body to cellular biodistribution of clinical-stage PEG-b-pHPMA-based core-crosslinked polymeric micelles, J. Control. Release 328 (2020), https://doi.org/10.1016/j.jconrel.2020.09.046.
[35] R. Choe, A. Corlu, K. Lee, T. Durduran, S.D. Konecky, M. Grosicka-Koptyra, S. R. Arridge, B.J. Czerniecki, D.L. Fraker, A. Demichele, B. Chance, M.A. Rosen, A. G. Yodh, Diffuse optical tomography of breast cancer during neoadjuvant chemotherapy: a case study with comparison to MRI, Med. Phys. 32 (2005), https://doi.org/10.1118/1.1869612.
[36] M. Schweiger, S.R. Arridge, Comparison of two- and three-dimensional reconstruction methods in optical tomography, Appl. Opt. 37 (1998), https://doi.org/10.1364/ao.37.007419.